scientific reports

Check for updates

OPEN

Misrepresentation of thermal stability across different oxidation states of copper compounds by SCAN meta-GGA functionals

Soungmin Bae[1]✉, Noriyuki Egawa[2] & Hannes Raebiger[2]✉

The Strongly Constrained and Appropriately Normed (SCAN) meta-GGA (generalized gradient approximation) density functional and its regularized derivatives (e.g., SCAN and r^{2}SCAN) have been proposed as a post-standard exchange-correlation functional, and are widely believed to replace conventional GGA functionals (e.g. PBE-GGA) owing to greatly improved electronic structures of strongly correlated systems and overall accuracy of total energies. While these improvements have been widely demonstrated for various systems, we report a significant failure of SCAN functionals related to erroneous stability of multivalent states of copper: SCAN and its derivatives (r^{2}SCAN) critically fail to predict the relative stability of copper in oxidation states Cu^{+1}(d^{10}) and Cu^{+2}(d^9), excessively stabilizing Cu^{+2} over Cu^{+1}, which leads to wrong relative stability of Cu_2O and CuO. This spurious bias also results in unphysical oxygen defect structures of $YBa_2Cu_3O_{7-\delta}$ for small δ. While the PBE-GGA functional can be fixed with a simple Hubbard-U correction (PBE + U) to predict both the spectral and thermochemical properties of copper compounds correctly, this is shown to not be the case for SCAN functionals. Our work advocates careful consideration of SCAN meta-GGA functionals when they are applied for cuprate superconductors, catalysis, and defect studies of copper compounds.

Strongly correlated materials are the Achilles heel of density-functional theories, where widely used local-density approximation (LDA) and generalized gradient approximation (GGA) fail to open up a band gap and correctly describe localized electrons. These failures are due to the self-interaction error, which tends to overly delocalize electrons in LDA and GGA. The Strongly Constrained and Appropriately Normed (SCAN) functional[1], a meta-GGA functional offers at least a partial solution to this problem by correctly opening up band gaps for Mott and charge transfer insulators[2–5] and cuprate superconductors[6–9]. In addition to the SCAN, recently developed regularized derivatives (e.g., r^{2}SCAN) exhibit similar accuracy as the SCAN functional but with improved numerical stability[10–15].

Hubbard-U corrections offer an alternative, albeit parametrized, means to correct for the shortcomings of LDA or GGA, which also have been widely used for Mott and charge transfer insulators[16–19], as well as for cuprate superconductors[20–24]. The shortcoming of Hubbard-U corrections is that U is an external parameter, and it is not clear how to determine its value, while SCAN meta-GGA functionals are parameter-free.

A known shortcoming of SCAN is its overcorrection for delocalized systems, that is, gaps are opened where there should be none, and spurious electron localization causes unphysical symmetry breakings and magnetizations. For example, SCAN predicts an antiferromagnetic insulator ground state for graphene instead of the well-known non-magnetic semi-metallic Dirac cone bands, and a symmetry-broken antiferromagnetic ground state for benzene[25]. Similar overstabilization of magnetic phase are also manifested by exaggerated magnetic momenta in ferromagnetic metals (Fe, Co, and Ni) and some magnetic compounds[26–28]. Also, SCAN predicts incorrectly the ground states of Ce-, Mn-, and Fe-based oxides, which however can be improved using SCAN + U.[29] In addition, Long et al. show that oxidation enthalpies for several transition metal oxides can be improved using SCAN + U, with the exception of copper oxides, where Hubbard-U corrections offer no improvement over SCAN[23,24,28,30] Similar behaviors were also observed with r^{2}SCAN + U functionals for copper and chromium oxides[31]. Thus, SCAN functionals would be prone to problems in several delocalized systems and transition metal oxides, and may also have problems in copper compounds i.e., SCAN functionals seems to be

[1]Institute for Materials Research, Tohoku University, 2-1-1 Katahira, Aoba-ku, Sendai 980-8577, Japan. [2]Department of Physics, Yokohama National University, Yokohama 240-8501, Japan. ✉email: bae.soungmin.d6@tohoku.ac.jp; hannes@ynu.ac.jp

able to describe well CuO with valence Cu^{2+} similar to that of many cuprate superconductors, but it is not clear whether it can describe well the valence of non-magnetic Cu^{+} such as Cu_2O.

Yttrium-based cuprates, namely, $YBa_2Cu_3O_{7-\delta}$ (YBCO) with $\delta = 0 \sim 1$, are particularly interesting superconductors due to their high transition temperature, and the multivalence of copper. Copper in YBCO has two different lattice positions (sites Cu_{edge} and Cu_{plane} shown in Fig. 1); in $YBa_2Cu_3O_7$ (YBCO7) copper on either site is in the Cu^{2+} state, whereas in $YBa_2Cu_3O_6$ (YBCO6) Cu_{edge} is in the Cu^{+} state, and Cuplane is in the Cu^{2+} state. Figure 1 shows the structure of YBCO6 and YBCO7. Oxygen has three sites (O_{plane}, O_{chain}, and O_{apical} shown in Fig. 1). All of the oxygen O in the chain site (O_{chain}) of YBCO7 is removed to form YBCO6, and the valence of Cu changes accordingly, being Cu^{+} in YBCO6. It has been observed that oxygen vacancies in $YBa_2Cu_3O_{7-\delta}$ (YBCO) are predominantly formed at the chain site O_{chain}[32–34], but also occur at the apical site O_{apical}[35,36], both of which are considered important for understanding the superconducting properties of YBCO. Considering these facts, there is need for a density functional that can consistently describe different valences and correctly predict the sites of oxygen vacancies in YBCO.

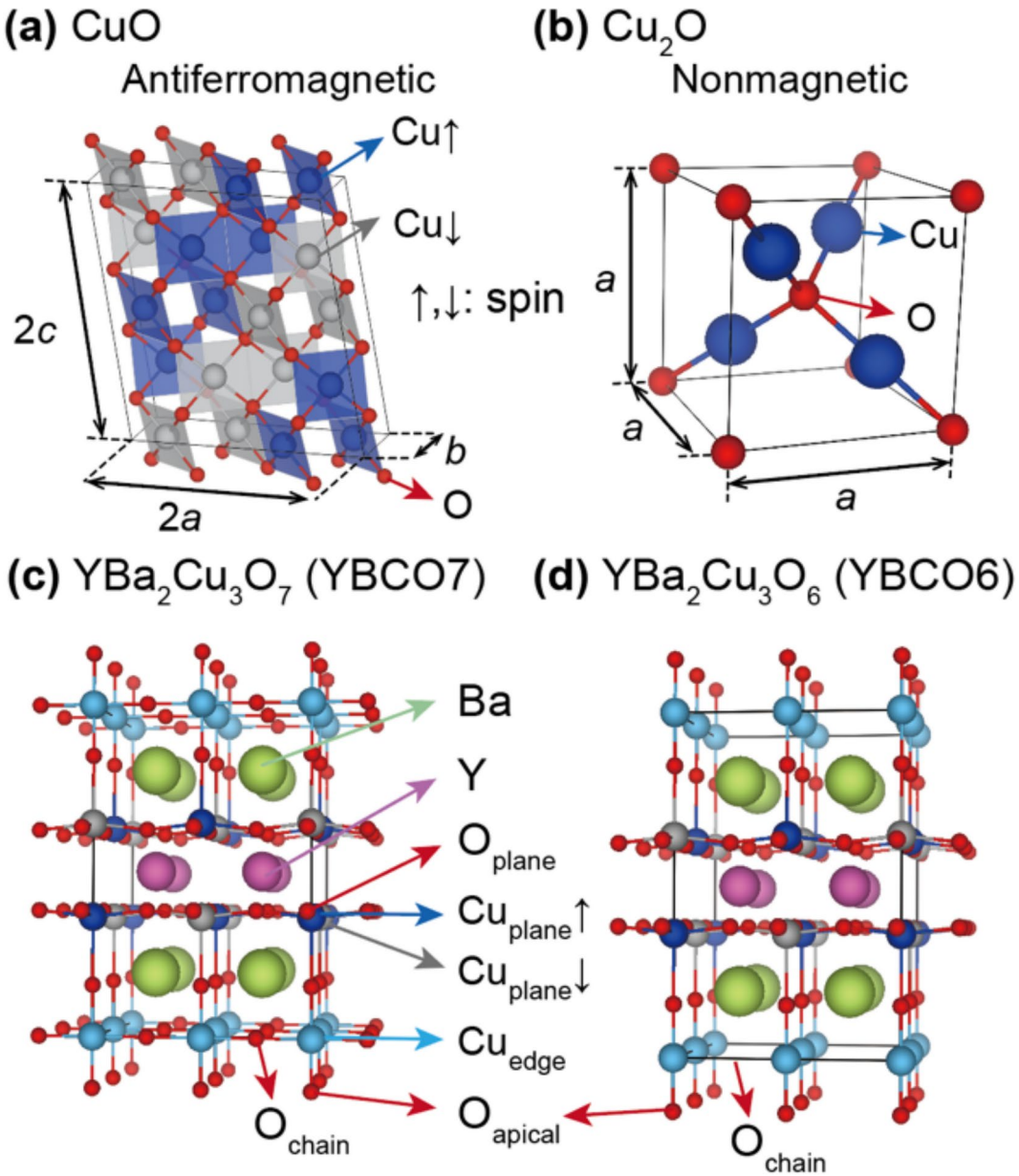

Fig. 1. Lattice structures of (**a**) CuO, (**b**) Cu_2O, (**c**) $YBa_2Cu_3O_6$ (YBCO6) and (**d**) $YBa_2Cu_3O_7$ (YBCO7). The arrows of Cu atoms indicate the local magnetic momenta in antiferromagnetic configurations. Three oxygen sites O_{plane}, O_{chain}, O_{apcial} and two copper sites Cu_{plane} and Cu_{edge} in YBCO7 and YBCO6 are categorized. It is noted that removing the oxygens in the O_{chain} sites in YBCO7 , gives rise to the oxygen-deficient structure of YBCO6.

In this work, we test the reliability of PBE, SCAN, and r^{2}SCAN functionals with a Hubbard-U correction (PBE + U, SCAN + U, and r^{2}SCAN + U) in CuO, Cu_2O and YBCO. We show that the stability of the two copper oxides can be reproduced in PBE + U, but Cu_2O is always unstable in SCAN and SCAN + U as well as in r^{2}SCAN and r^{2}SCAN + U. In addition, we show that SCAN and SCAN + U, unlike PBE + U, prefer excessively apical vacancy formation , which is not consistent with the experiment. This similar behavior was also observed for r^{2}SCAN and r^{2}SCAN + U.

Results and discussion

The cupric oxide (CuO)[37] and the nonmagnetic cuprous oxide (Cu_2O)[38] are illustrated in Fig. 1a, b. The formal oxidation state of Cu atoms in CuO and Cu_2O are Cu^{+2} and Cu^{+1}, resulting in the antiferromagnetism and nonmagnetism of CuO and Cu_2O stemming from spin-polarized and spin-unpolarized d^9 and d^{10} electron configurations. YBCO7 ($YBa_2Cu_3O_7$) and YBCO6 ($YBa_2Cu_3O_6$) are shown in Fig. 1c, d, which contain different sites of copper (Cu) and oxygen (O) atoms i.e., Cu_{plane} and Cu_{edge} for Cu atoms and O_{plane}, O_{chain}, and O_{apical} for O atoms. By removing O_{chain} atoms from YBCO7, the valence of Cu_{edge} changes into Cu^+, therefore YBCO6 contains both Cu^+ and Cu^{2+} at Cu_{edge} and Cu_{plane}, respectively. This implies that the phase stability of Cu_2O and CuO with Cu^+ and Cu^{2+} should be intimately related to the reduction reaction of YBCO7, involving the transition of oxidation state of Cu_{edge} atoms Cu^{2+} to Cu^+. Tables 1 and 2 compare the optimized lattice parameters and local magnetic moment of CuO, Cu_2O, YBCO6, and YBCO7 obtained from PBE + U, SCAN, and r^{2}SCAN functionals to the experimental values[31,32,35–41] and shows generally good agreement between experiment and calculation.

The chemical stability of CuO and Cu_2O explicitly depends on chemical potentials of copper and oxygen, and the predictability of the relative stability of these competing phases has been a bolometer for benchmarking approximate exchange-correlation functionals of DFT calculations[22–24,28–30,38,42]. At zero pressure and zero temperature, the formation enthalpy of CuO and Cu_2O are calculated as

$$\Delta H_{\mathrm{f}}(\mathrm{CuO}) = E(\mathrm{CuO}) - {\mu_{\mathrm{Cu}}}^0 - {\mu_{\mathrm{O}}}^0, \tag{1}$$

$$\Delta H_{\mathrm{f}}(\mathrm{Cu_2O}) = E(\mathrm{Cu_2O}) - 2{\mu_{\mathrm{Cu}}}^0 - {\mu_{\mathrm{O}}}^0, \tag{2}$$

where E(CuO) and E(Cu_2O) are the total energies per formula unit of CuO and Cu_2O, ${\mu_{\mathrm{Cu}}}^0$ and ${\mu_{\mathrm{O}}}^0$ are the reference chemical potentials of single Cu and O atoms, which are evaluated from total energies of the Cu metal and the spin-triplet state O_2 molecule. At finite temperatures and varying pressures, the chemical potentials of Cu and O change from the reference chemical potentials as $\mu_i = \mu_i^0 + \Delta\mu^i$ (i = Cu, O), and the changes in $\Delta\mu^i$ are bound by the following relationships,

$$\Delta H_{\mathrm{f}}(\mathrm{CuO}) = \Delta\mu_{\mathrm{Cu}} + \Delta\mu_{\mathrm{O}}, \tag{3}$$

$$\Delta H_{\mathrm{f}}(\mathrm{Cu_2O}) = \Delta\mu_{\mathrm{Cu}} + 2\Delta\mu_{\mathrm{O}}. \tag{4}$$

Figure 2 shows the phase stability of CuO and Cu_2O predicted with DFT calculations employing PBE + U, SCAN + U and r^{2}SCAN + U functionals. The gray zone in Fig. 2a–e shows the area with $\Delta\mu_i > 0$ where the formation of the Cu metal and O_2 molecule are thermally preferred compared to the formation of CuO and

	PBE + U	SCAN	r^2SCAN	Experiment[31,32,35–37]
CuO				
a (Å)	4.468	4.340	4.588	4.684
b (Å)	3.766	3.809	3.428	3.423
c (Å)	5.195	5.151	5.088	5.190
β (°)	90.77	92.01	99.29	99.54
d (Å)	1.955	1.938	1.941	1.96
V (Å^3)	87.39	85.09	78.97	81.08
m (μ_B)	0.60	0.54	0.54	0.68
E_g (eV)	1.23	0.75	0.46	1.35
ΔH_f (eV)	−1.40	−1.55	−1.56	−1.62
Cu_2O				
a (Å)	4.291	4.244	4.288	4.270
d (Å)	1.858	1.838	1.856	1.85
V (Å^3)	79.04	76.46	78.83	77.83
E_g (eV)	0.68	0.83	0.83	2.17
ΔH_f (eV)	−1.57	−1.55	−1.57	−1.77

Table 1. Lattice constants, volumes, band gaps, and formation enthalpies of CuO and Cu_2O obtained from experiments[37–41]and first-principles calculations with PBE + U (U_{eff} = 5 eV), SCAN, and R^{2}SCAN functionals including lattice constants (a, b, and c), local magnetic moment m, band gap E_g, formation enthalpy ΔH_f, and the bond length d between Cu and O.

	PBE + U	SCAN	r^2SCAN	Experiment[35]
YBCO6 ($YBa_2Cu_3O_6$)				
a (Å)	3.876	3.85	3.86	3.87
c (Å)	12.071	11.92	11.93	11.74
V (Å^3)	181.32	176.55	177.49	175.94
$d(Cu_{edge}–O_{apical})$ (Å)	1.815	1.80	1.80	1.81
$d(Cu_{plane}–O_{apical})$ (Å)	2.570	2.52	2.53	2.42
$d(Cu_{plane}–O_{plane})$ (Å)	1.950	1.94	1.94	1.95
YBCO7 ($YBa_2Cu_3O_7$)				
a (Å)	3.86	3.83	3.83	3.83
b (Å)	3.91	3.87	3.88	3.88
c (Å)	11.88	11.66	11.68	11.68
V (Å^3)	179.18	172.71	173.98	173.55
$d(Cu_{edge}–O_{chain})$ (Å)	1.953	1.93	1.94	1.94
$d(Cu_{edge}–O_{apical})$ (Å)	1.847	1.86	1.86	1.83
$d(Cu_{plane}–O_{apical})$ (Å)	2.421	2.23	2.27	2.32
$d(Cu_{plane}–O_{plane})$ (Å)	1.946	1.95	1.95	1.93

Table 2. Lattice constants of and bond lengths of YBCO6 ($YBa_2Cu_3O_6$) and YBCO7 ($YBa_2Cu_3O_7$) obtained with PBE + *U* (U_{eff} = 5 eV), SCAN, and R^{2}SCAN functionals compared to experimental values. [35 39]

Cu_2O, which means that the chemical potentials are only allowed to vary in the negative quadrant $\Delta\mu_i < 0$. In Fig. 2, the filled and open circles represent the experimental and calculated intersection points of Eqs. 3 and 4, which represent the chemical environment in which CuO and Cu_2O coexist in equilibrium. To the left from the intersection point Cu_2O is stable, and to the right CuO. As shown in Fig. 2a, b, PBE gives the intersection point in the allowed area ($\Delta\mu_i < 0$) and PBE + *U* (U_{eff} = 8 eV) closely reproduces the experimentally observed relative stabilities of Cu_2O and CuO, which indicates that the Hubbard-*U* correction on Cu-3*d* states can improve the accuracy of the formation enthalpies and phase stability of CuO and Cu_2O. In contrast, an opposite behavior is observed in SCAN functional as shown in Fig. 2c, d; SCAN gives the intersection point in the prohibited region ($\Delta\mu_i > 0$), which is seemingly caused by a biased energetic preference of SCAN for partially occupied states compared to fully occupied states as previously reported,[19–21,25–27] leading to overstabilization of CuO (Cu^{2+}, d^9) compared to Cu_2O (Cu^+, d^{10}). It is important to remark that the absolute values of the SCAN formation enthalpies are much closer to the experimental values than the PBE ones, but for CuO and Cu_2O, the errors have opposite signs: there is an overbinding for CuO and an underbinding for Cu_2O. Thus, even though the quantitative errors are small, the opposite signs make the error *qualitative*, such that per SCAN, Cu_2O is predicted unstable. The Hubbard-*U* correction on SCAN functional does not improve the relative phase stability of CuO and Cu_2O but instead, leads to further stabilization of CuO with a partially occupied d^9 state. This is because the Hubbard-*U* correction only improves the underbinding of Cu_2O but *worsens* the overbinding of CuO. The overall behavior of PBE + *U* and SCAN + *U* functional for a wide range of U_{eff} parameter is demonstrated in Fig. 2e, which shows that the correct phase stability of CuO and Cu_2O cannot be achieved with SCAN + *U* functional with a positive U_{eff} parameter. While r^{2}SCAN functionals also exhibit similar overstabilization of CuO over Cu_2O, the error is relatively modest compared to SCAN as the intersection point (i.e., the equilibrium chemical potential) in the phase space is closer to the experimental value. Importantly, r^{2}SCAN brings the intersection point of CuO and Cu_2O formation enthalpies into the negative quadrant in the phase space, i.e., r^{2}SCAN recovers the chemical stability of Cu_2O. We note that a negative U_{eff} parameter also might be adopted in SCAN + *U* and r^{2}SCAN + *U* functionals, however applying such corrections result in severe band gap underestimation of Cu_2O. Previous works[28] also reported that SCAN and r^{2}SCAN without Hubbard-*U* correction (U_{eff} = 0.0 eV) would be the optimal choice to obtain least errors of the formation enthalpy of CuO and Cu_2O[28,31]. The SCAN functionals with nonlocal van der Waals corrections (SCAN + rVV10[43] and r^{2}SCAN + rVV10[44]) were also tested, showing no significant effect on the results (see Supplementary Information).

By comparing the densities of states and experimental ultraviolet photoemission spectroscopy (UPS) spectra[45], we examined the predictive power of each functional for the valence band structures of CuO and Cu_2O in Fig. 3. Figure 3a shows the UPS spectra and densities of states (DOS) that were obtained using the PBE, PBE + *U* (U_{eff} = 5 eV and 8 eV), SCAN and r^{2}SCAN functionals. The primary UPS peak at around 3 eV is attributed to Cu-3*d* states through comparison of the UPS spectrum and DOS of CuO. Cu-3*d* states become deeper as U_{eff} parameter of PBE + *U* increases, PBE + *U* (U_{eff} = 5 eV) gives the closest Cu-3*d* position compared with the experimental UPS spectrum, whereas the U_{eff} = 8 eV giving the optimal thermal stability of CuO and Cu_2O shifts the Cu-3*d* position to too low energies. This suggests that a PBE + *U* (U_{eff} = 5 eV) might be a reasonable compromise for both the electronic spectrum (the valence band structure) and formation enthalpies. While SCAN and r^{2}SCAN obtain similar valance band structures compared to the experimental UPS spectra, they predict the erroneous phase stability of CuO and Cu_2O (cf. Figure 2). The similar behavior of the position of Cu-3*d* states is also shown for Cu_2O in Fig. 3b; the density of states obtained with PBE + *U* (U_{eff} = 5 eV) optimally reproduces the main peak of the experimental UPS spectrum around −3 eV. It is shown that the band gap of Cu_2O is less sensitive to the choice of the functional and *U* parameter, unlike the band gap of CuO, which is a

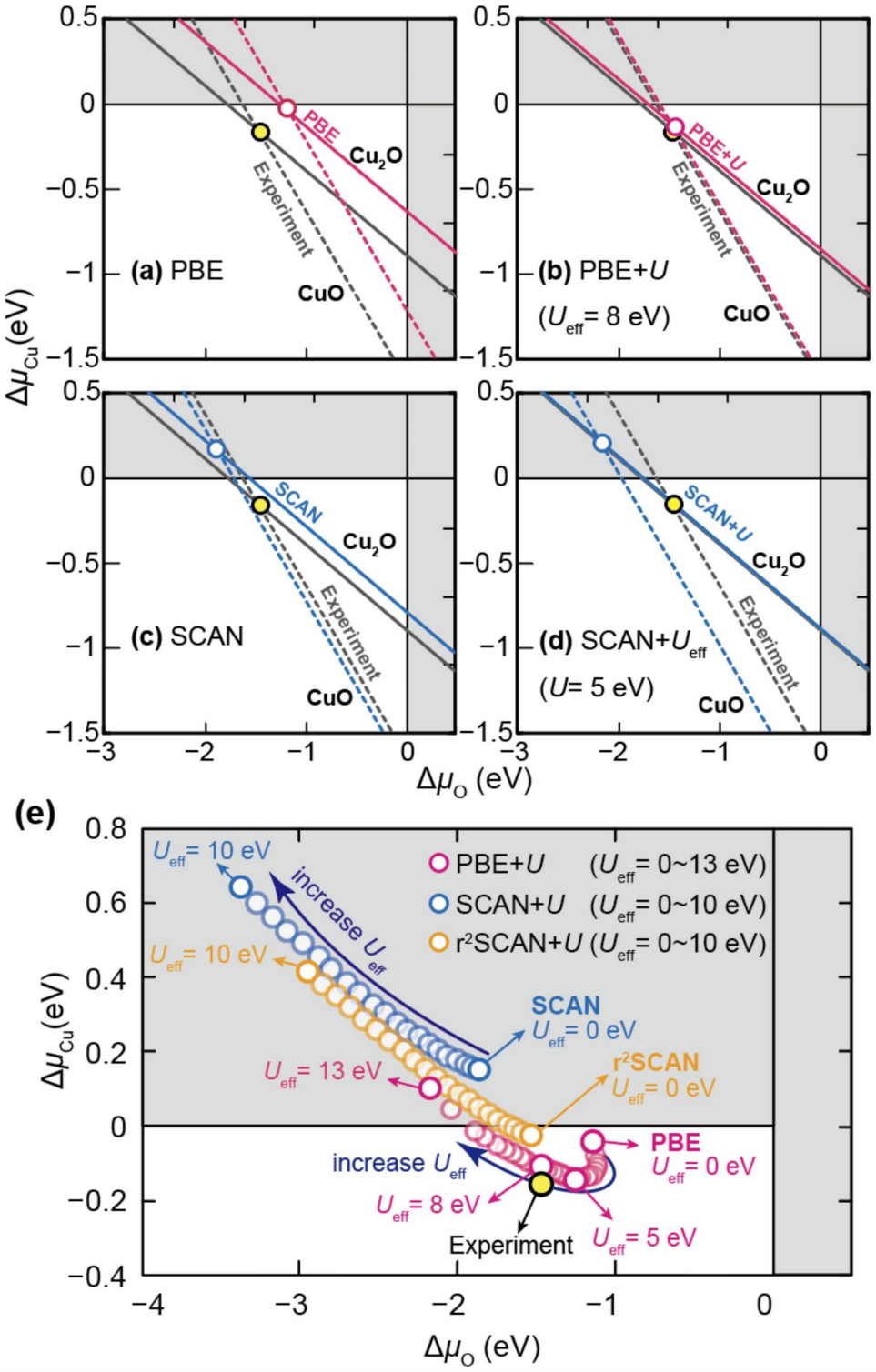

Fig. 2. The phase stability of CuO and Cu_2O as function of chemical potential obtained with experiment and DFT calculations with PBE + U and SCAN + U functionals. The phase stabilities with (**a**) PBE, (**b**) PBE + U (U_{eff} = 8 eV), (**c**) SCAN, and (**d**) SCAN + U (U_{eff} = 5 eV). The circles denote intersection points where the relative stability of CuO and Cu_2O changes. (**e**) The U_{eff} parameter dependence of the intersection points predicted by PBE + U, SCAN + U and r^{2}SCAN + U functionals.

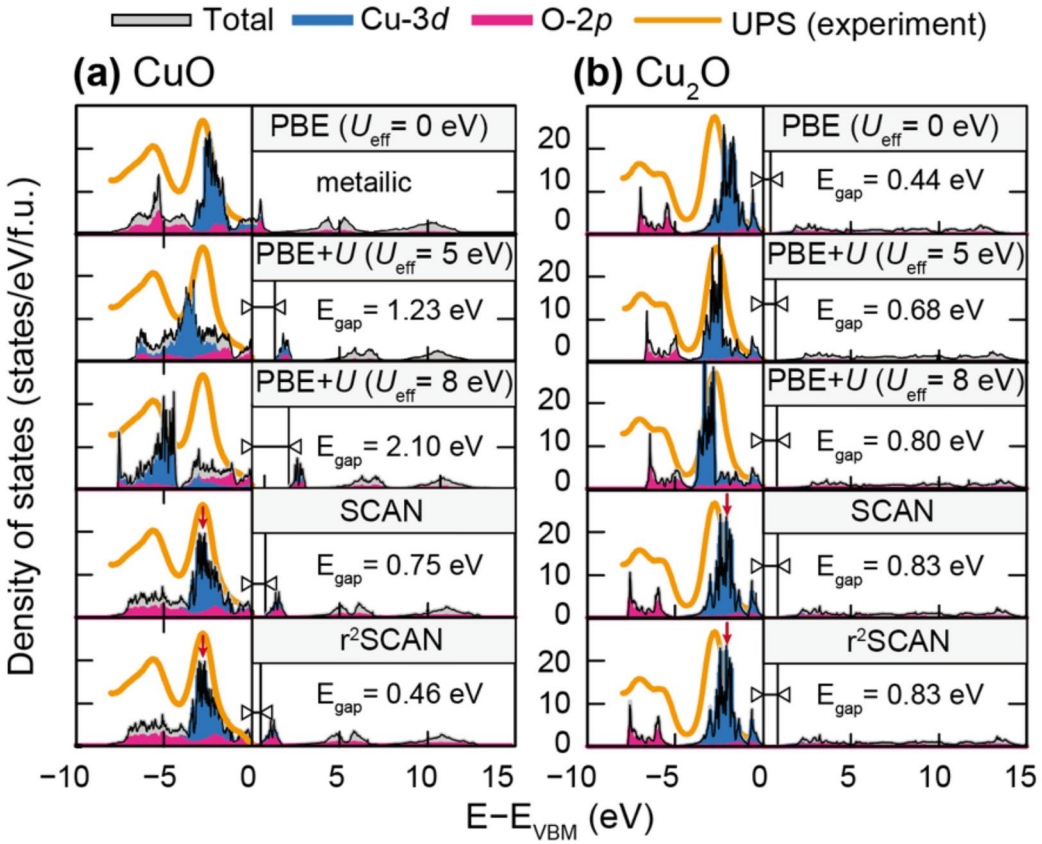

Fig. 3. Densities of states of CuO and Cu_2O obtained with PBE, PBE + U (U_{eff} = 5 eV, and 8 eV), SCAN, and r^{2}SCAN functionals compared to experimental spectra of ultraviolet photoemission spectroscopy (UPS) of Ref.[45].

d–d gap originated from the partially occupied $3d^9$ states and strongly influenced by the choice of Hubbard-U parameter and the type of functional[46].

YBCO7 and YBCO6 have two distinct Cu_{plane} and Cu_{edge} sites (cf. Figure 1c, d), the valence of Cu_{edge} atoms is expected to be directly changed from Cu^{2+} to Cu^{+} as YBCO7 becomes YBCO6 by removing oxygen atoms at O_{chain}. As SCAN functional has been found to give an erroneous phase stability of CuO and Cu_2O with $Cu^{+}(d^9)$ and Cu^{2+} (d^{10}) due to a spurious energetical preference for partially filled d^9 states, the oxygen vacancy formations of YBCO7 seems to be also prone to such a bias of SCAN and r^{2}SCAN functionals.

Notably, it has been confirmed that oxygen vacancies are predominantly formed at the O_{chain} site compared to the O_{apical} site[32–34], with both types of oxygen vacancies being experimentally verified[35,36]. For obtaining the proper description of oxygen-deficient YBCO, we calculate the oxygen vacancies at O_{chain} and O_{apical} in YBCO7 with PBE + U (U_{eff} = 5 eV) SCAN and r^{2}SCAN functionals to investigate the bias of SCAN meta-GGA functionals in oxygen vacancy formation in YBCO.

The formation energy of oxygen vacancy in YBCO7 is calculated as $E_f = E(V_O) + \mu_O{}^0 - E(\text{YBCO7})$, where $E(V_O)$ is the total energy of $YBCO_{7-\delta}$ containing an oxygen vacancy (V_O), $\mu_O{}^0$ is the reference chemical potential of oxygen defined as the half of the total energy of the oxygen molecule in the triplet spin state $\mu_O{}^0 = 1/2E(O_2)$, and E(YBCO7) is the total energy of pristine YBCO7 supercell. Figure 4a shows the formation energies of V_O at the O_{apical} and O_{chain} in $YBCO_{7-\delta}$ at two concentrations $\delta = 0.0625$ and 0.125 calculated with PBE, PBE + U (U_{eff} = 5 eV), and SCAN functionals. Whereas PBE and PBE + U predict a higher formation enthalpy of V_O at the O_{apical} compared to V_O at the O_{chain}, SCAN and r^{2}SCAN predict that V_O at the O_{apical} is more stable in contrast to PBE and PBE + U. This contrasting tendency of SCAN functional is originated from the spuriously biased total energy of $Cu^{+}(d^9)$ and $Cu^{+}(d^{10})$ configurations, leading to an inconsistent description compared to experimental observations[32–34].

We next look at the bond lengths given for the YBCO6.875 with a single oxygen vacancy (V_O) at the O_{apical} and O_{chain} sites in Fig. 4b. Oxygen vacancies cause electron doping of YBCO, which should provide electrons to neighboring Cu atoms. Indeed, neighboring Cu atoms at Cu_{edge} sites with a $Cu^{2+}(d^9)$ configuration are electron-doped into a $Cu^{+}(d^{10})$-like configuration, as shown by local distortion of bond lengths surrounding V_O, manifested by strongly shrinking Cu-O bonds. As illustrated in Fig. 4b, the bond length shrinking between Cu-O atoms can be attributed to a transition from $Cu^{2+}(d^9)$ to $Cu^{+}(d^{10})$, based on comparison wirh Cu-O bond lengths in CuO (d^9) and Cu_2O (d^{10}) of 1.95 Å and 1.86 Å, respectively. While the V_O at O_{apcial} site displaces one neighbor Cu atom by providing electrons, the V_O at O_{chain} site displaces two surrounding Cu atoms, which

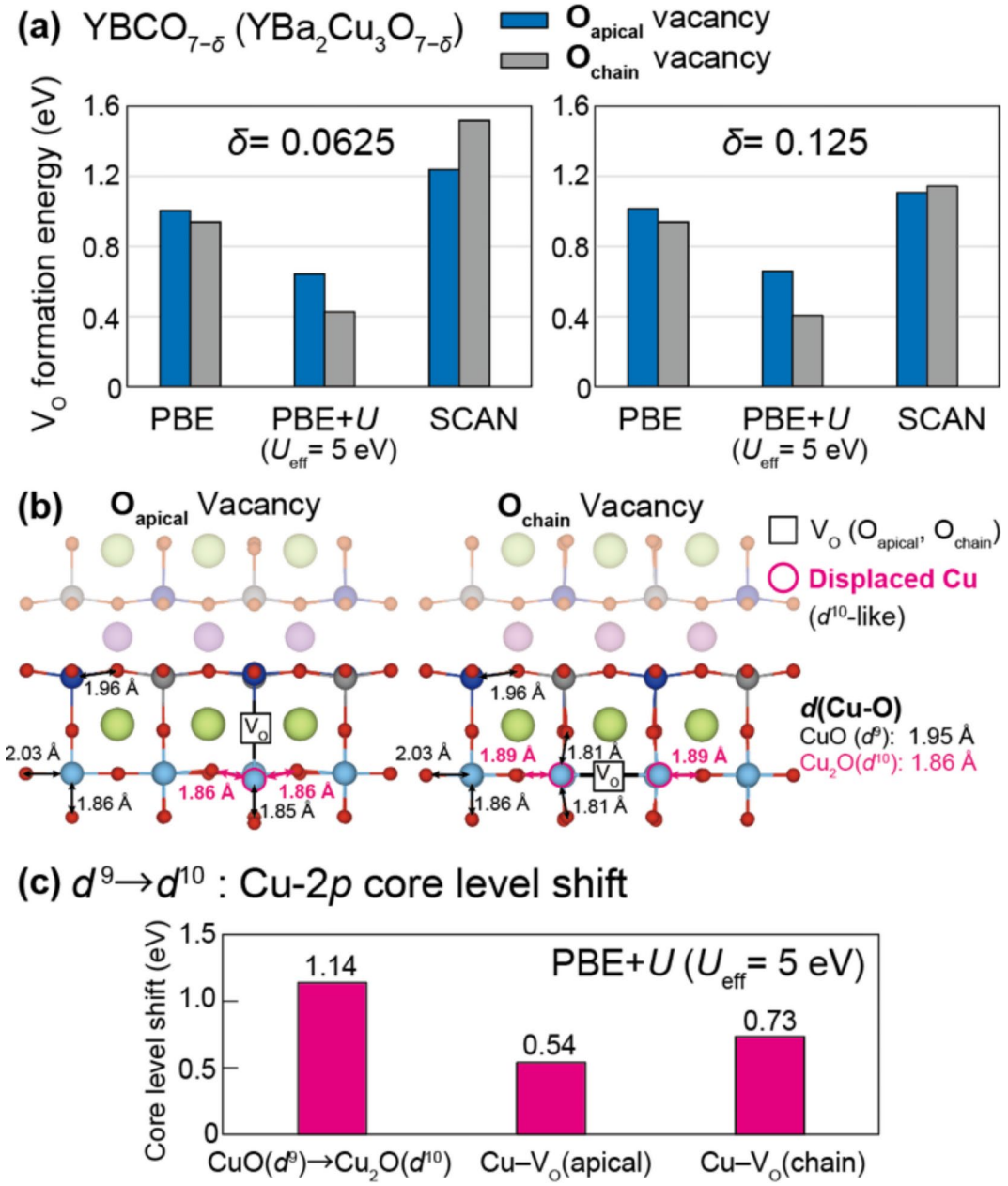

Fig. 4. Oxygen vacancies in YBCO7. (**a**) Formation energies of the oxygen vacancy at O_{apical} and O_{chain} sites in $YBCO_{7-\delta}$ with $\delta = 0.0625$ and 0.125 calculated with PBE, PBE + U (U_{eff} = 5 eV), and SCAN functionals. (**b**) Local atomic structures of $YBCO_{6.875}$ around oxygen vacancies at O_{apical} and O_{chain} sites. Bond lengths between Cu and O atoms d(Cu-O) are compared with the bond lengths of CuO (d^9) and Cu_2O (d^{10}). (**c**) Calculated Cu-2p core level shifts from $d^9 \rightarrow d^{10}$ transition introduced by the oxygen vacancies compared with the core level shifts from CuO (d^9) and Cu_2O (d^{10}).

means the V_O at O_{chain} site more strongly drives the reduction from $Cu^{2+}(d^9)$ to $Cu^{+}(d^{10})$ compared to the V_O at O_{apical} site. This is in line with the observed phase stability of CuO and Cu_2O, where SCAN and r^{2}SCAN overly stabilize CuO (d^9) against Cu_2O (d^{10}).

Figure 4c shows the calculated core level shift of Cu-2p compared between Cu-d^9 Cu-d^{10} configurations calculated by PBE + U (U_{eff} = 5 eV). As demonstrated in the core level shift from CuO (d^9) to Cu_2O (d^{10}), providing electrons into d^9 states results in a positive core level shift (i.e., weakening the binding energy of core electrons), which is due to an enhanced electron screening effect with more valence electrons in 3d states. Oxygen vacancies at O_{apical} and O_{chain} sites also induce positive core level shifts in the Cu-2p state, which indicates an effective the d^9 to d^{10} transition of neighboring (displaced) Cu atoms around oxygen vacancies (V_O). Since the V_O at O_{chain} site induces larger core level shifts compared to the V_O at O_{apical} site, this further clarifies the increased d^{10} character of the V_O at O_{chain} which is evaluated as more unstable than the V_O at O_{apical} by SCAN functionals.

In summary, we clarify a systematic failure of SCAN meta-GGA density-functionals (SCAN and r^{2}SCAN), which spuriously stabilizes the $Cu^{2+}(d^9)$ configurations rather than the $Cu^{+}(d^{10})$ configurations. This bias leads to the failure to stabilize Cu_2O at any allowed chemical potential for the SCAN functionals, while PBE-GGA functional with a Hubbard-U correction reasonably reproduces the experimental relative phase stability of CuO and Cu_2O. Meanwhile, both PBE + U and SCAN functionals predict the valence band structures of CuO and Cu_2O well in agreement with the ultraviolet photoemission spectroscopy (UPS) spectra. The energetic bias of SCAN functionals on d^9 and d^{10} configurations results in different relative stability of oxygen vacancies in YBCO7 at O_{apical} and O_{chain} sites: SCAN functionals prefers O_{chain} vacancies as opposed to PBE and PBE + U functionals, which contradicts a series of experimental observations[32–34]. This work confirms a systematic bias in the SCAN meta-GGA functional regarding the energetics of partially and fully occupied 3d states, as observed by the overstabilization of spin-polarized states in various compounds[26–28]. Addressing this bias is essential for providing accurate predictions for copper-based compounds, particularly those containing Cu^+ and Cu^{2+} states.

Methods

The first principles calculations were performed by using density-functional theory (DFT) with the projected augmented-wave (PAW) method as implemented in the VASP package[47–49]. The kinetic cutoff energy was set to 500 eV. The calculations were carried out with PBE-GGA[50], SCAN[11], and r^{2}SCAN[10] exchange correlation functionals and SCAN functionals with the revised VV10 kernel[51] (SCAN + rVV10[43] and r^{2}SCAN + rVV10[44]) with applying the Hubbard-U correction on the Cu-3d states based on Dudarev's method[52]. The antiferromagnetic cupric oxide CuO (tenorite)[37] and the nonmagnetic cuprous oxide Cu_2O (cuprite)[38] were calculated by using DFT with $7\times10\times7$ and $8\times8\times8$ $\boldsymbol{k}$-point grids generated with the Monkhorst-Pack meshes[53]. The $YBa_2Cu_3O_7$ (YBCO7) and $YBa_2Cu_3O_6$ (YBCO6) were calculated within antiferromagnetic configurations sampled with the $4\times4\times3$ $\boldsymbol{k}$-point grids. Oxygen vacancies at chain and apical sites (O_{chain} and O_{apcial}, see Fig. 1) in YBCO7 were simulated using the supercell approach adopting $4\times4\times1$, and $2\times2\times1$ supercells, which correspond to $YBCO_{6.9375}$, and $YBCO_{6.875}$, respectively. Cu-2p core levels are evaluated from a postprocess of DFT results with PAW method with an initial state approximation, as implemented in the VASP package[54].

Data availability

The data that support the findings of this study are available from the corresponding author upon reasonable request.

Received: 7 October 2024; Accepted: 25 February 2025
Published online: 04 March 2025

References

1. Sun, J., Ruzsinszky, A. & Perdew, J. P. Strongly constrained and appropriately normed semilocal density functional. *Phys. Rev. Lett.* **115**, 036402. https://doi.org/10.1103/PhysRevLett.115.036402 (2015).
2. Zhang, Y. et al. Symmetry-breaking polymorphous descriptions for correlated materials without interelectronic *U*. *Phys. Rev. B.* **102**, 045112. https://doi.org/10.1103/PhysRevB.102.045112 (2020).
3. Varignon, J., Bibes, M. & Zunger, A. Mott gapping in 3d ABO_3 perovskites without Mott-Hubbard interelectronic repulsion energy *U*. *Phys. Rev. B.* **100**, 035119. https://doi.org/10.1103/PhysRevB.100.035119 (2019).
4. Zayed, M. K., Elabbar, A. A. & Yassin, O. A. Electronic and optical properties of the VO2 monoclinic phase using SCAN meta-GGA and TB-mBJ methods. *Phys. B Condens. Matter*. **582**, 411887. https://doi.org/10.1016/j.physb.2019.411887 (2020).
5. Mondal, W. R. et al. Role of V-V dimers on structural, electronic, magnetic, and vibrational properties of VO_2 by first-principles simulations and Raman spectroscopic analysis. *Phys. Rev. B.* **103**, 214107. https://doi.org/10.1103/PhysRevB.103.214107 (2021).
6. Lane, C. et al. Antiferromagnetic ground state of La_2CuO_4: a parameter-free Ab initio description. *Phys. Rev. B.* **98**, 125140. https://doi.org/10.1103/PhysRevB.98.125140 (2018).
7. Zhang, Y. et al. Competing stripe and magnetic phases in the cuprates from first principles. *Proc. Natl. Acad. Sci. U. S. A.* **117**, 68 (2020). https://doi.org/10.1073/pnas.1910411116
8. Nokelainen, J. et al. Ab initio description of the $Bi_2Sr_2CaCu_2O_{8+\delta}$ electronic structure. *Phys. Rev. B.* **101**, 214523. https://doi.org/10.1103/PhysRevB.101.214523 (2020).
9. Pokharel, K. et al. Sensitivity of the electronic and magnetic structures of cuprate superconductors to density functional approximations. *Npj Comput. Mater.* **8** https://doi.org/10.1038/s41524-022-00711-z (2022).
10. Furness, J. W., Kaplan, A. D., Ning, J., Perdew, J. P. & Sun, J. Accurate and numerically efficient r2SCAN meta-generalized gradient approximation. *J. Phys. Chem. Lett.* **11**, 8208. https://doi.org/10.1021/acs.jpclett.0c02405 (2020).
11. Kingsbury, R. S. et al. A flexible and scalable scheme for mixing computed formation energies from different levels of theory. *Npj Comput. Mater.* **8**, 195. https://doi.org/10.1038/s41524-022-00881-w (2022).
12. DelloStritto, M. J., Kaplan, A. D., Perdew, J. P. & Klein, M. L. Predicting the properties of NiO with density functional theory: impact of exchange and correlation approximations and validation of the r2SCAN functional. *APL Mater.* **11** https://doi.org/10.1063/5.0146967 (2023).
13. Kothakonda, M. et al. Testing the r2SCAN density functional for the thermodynamic stability of solids with and without a Van der Waals correction. *ACS Mater. Au*. **3**, 102. https://doi.org/10.1021/acsmaterialsau.2c00059 (2023).
14. Kingsbury, R. et al. Performance comparison of r2SCAN and SCAN MetaGGA density functionals for solid materials via an automated, high-throughput computational workflow. *Phys. Rev. Mater.* **6**, 013801. https://doi.org/10.1103/PhysRevMaterials.6.013801 (2022).
15. Ning, J. et al. Comparing first-principles density functionals plus corrections for the lattice dynamics of $YBa_2Cu_3O_6$. *J. Chem. Phys.* **160** https://doi.org/10.1063/5.0181349 (2024).
16. Trimarchi, G., Wang, Z. & Zunger, A. Polymorphous band structure model of gapping in the antiferromagnetic and paramagnetic phases of the Mott insulators MnO, FeO, CoO, and NiO. *Phys. Rev. B.* **97** https://doi.org/10.1103/PhysRevB.97.035107 (2018).
17. Anisimov, V. V., Zaanen, J. & Andersen, O. K. Band theory and Mott insulators: Hubbard U instead of stoner *I*. *Phys. Rev. B.* **44**, 943. https://doi.org/10.1103/physrevb.44.943 (1991).
18. Cai, T. et al. Study on the ground state of NiO: the LSDA (GGA) + *U* method. *Phys. B Condens. Matter*. **404**, 89. https://doi.org/10.1016/j.physb.2008.10.009 (2009).

19. Heinemann, M., Eifert, B. & Heiliger, C. Band structure and phase stability of the copper oxides Cu_2O, CuO, and Cu_4O_3. *Phys. Rev. B.* **87**, 115111. https://doi.org/10.1103/PhysRevB.87.115111 (2013).
20. Anisimov, V. I. et al. Computation of stripes in Cuprates within the LDA + *U* method. *Phys. Rev. B.* **70**, 172501. https://doi.org/10.1103/PhysRevB.70.172501 (2004).
21. Pesant, S. & Côté, M. DFT + *U* study of magnetic order in doped La_2CuO_4 crystals. *Phys. Rev. B.* **84**, 085104. https://doi.org/10.1103/PhysRevB.84.085104 (2011).
22. Sterling, T. C. & Reznik, D. Effect of the electronic charge gap on LO bond stretching phonons in undoped La_2CuO_4 calculated using LDA + *U*. *Phys. Rev. B.* **104**, 134311. https://doi.org/10.1103/PhysRevB.104.134311 (2021).
23. Lopez, G. M., Filippetti, A., Mantega, M. & Fiorentini, V. First-principles calculation of electronic and structural properties of $YBa_2Cu_3O_{6+y}$. *Phys. Rev. B.* **82** https://doi.org/10.1103/PhysRevB.82.195122 (2010).
24. Murphy, S. T. A point defect model for $YBa_2Cu_3O_7$ from density functional theory. *J. Phys. Commun.* **4**, 115003. https://doi.org/10.1088/2399-6528/abc9a7 (2020).
25. Zhang, Y., Zhang, W. & Singh, D. J. Localization in the SCAN meta-generalized gradient approximation functional leading to broken symmetry ground States for graphene and benzene. *Phys. Chem. Chem. Phys.* **22**, 19585. https://doi.org/10.1039/d0cp03567j (2020).
26. Fu, Y. & Singh, D. J. Applicability of the strongly constrained and appropriately normed density functional to transition-metal magnetism. *Phys. Rev. Lett.* **121**, 207201. https://doi.org/10.1103/PhysRevLett.121.207201 (2018).
27. Fu, Y. & Singh, D. J. Density functional methods for the magnetism of transition metals: SCAN in relation to other functionals. *Phys. Rev. B.* **100**, 045126. https://doi.org/10.1103/PhysRevB.100.045126 (2019).
28. Long, O. Y., Carter, E. A. & G. S. G., and Evaluating optimal U for 3d transition-metal oxides within the SCAN + *U* framework. *Phys. Rev. Mater.* **4**, 045401. https://doi.org/10.1103/PhysRevMaterials.4.045401 (2020).
29. Gautam, G. S. & Carter, E. A. Evaluating transition metal oxides within DFT-SCAN and SCAN + *U* frameworks for solar thermochemical applications. *Phys. Rev. Mater.* **2**, 095401. https://doi.org/10.1103/PhysRevMaterials.2.095401 (2018).
30. Artrith, N., Garrido Torres, J. A., Urban, A. & Hybertsen, M. S. Data-driven approach to parameterize SCAN + *U* for an accurate description of 3d transition metal oxide thermochemistry. *Phys. Rev. Mater.* **6**, 035003. https://doi.org/10.1103/PhysRevMaterials.6.035003 (2022).
31. Swathilakshmi, S., Devi, R. & Sai Gautam, G. Performance of the r2SCAN functional in transition metal oxides. *J. Chem. Theory Comput.* **19**, 4202. https://doi.org/10.1021/acs.jctc.3c00030 (2023).
32. Kwok, W. K. et al. Electronic behavior of oxygen-deficient YBa2Cu3O7-δ. *Phys. Rev. B.* **37**, 106. https://doi.org/10.1103/physrevb.37.106 (1988).
33. Jorgensen, J. D. et al. Structural properties of oxygen-deficient YBa2Cu3O7- delta. *Phys. Rev. B Condens. Matter.* **41**, 1863. https://doi.org/10.1103/physrevb.41.1863 (1990).
34. Veal, B. W. et al. Time-dependent superconducting behavior of oxygen-deficient YBa2Cu3Ox: possible annealing of oxygen vacancies at 300 K. *Phys. Rev. B.* **42**, 4770. https://doi.org/10.1103/physrevb.42.4770 (1990).
35. Hartman, S. T. et al. Direct observation of apical oxygen vacancies in the high-temperature superconductor $YBa_2Cu_3O_{7-x}$. *Phys. Rev. Mater.* **3**, 114806. https://doi.org/10.1103/PhysRevMaterials.3.114806 (2019).
36. Mundet, B. et al. Local strain-driven migration of oxygen vacancies to apical sites in $YBa_2Cu_3O_{7-x}$. *Nanoscale* **12**, 5922. https://doi.org/10.1039/d0nr00666a (2020).
37. Forsyth, J. B., Brown, P. J. & Wanklyn, B. M. Magnetism in cupric oxide. *J. Phys. C: Solid State Phys.* **21**, 2917. https://doi.org/10.1088/0022-3719/21/15/023 (1988).
38. Neuburger, M. C. Präzisionsmessung der Gitterkonstante von Cuprooxyd Cu_2O. *Z. Physik.* **67**, 845. https://doi.org/10.1007/bf01390765 (1931).
39. Calestani, G. & Rizzoli, C. Crystal structure of the $YBa_2Cu_3O_7$ superconductor by single-crystal X-ray diffraction. *Nature* **328**, 606. https://doi.org/10.1038/328606a0 (1987).
40. Marabelli, F., Parravicini, G. B. & Salghetti-Drioli, F. Optical gap of CuO. *Phys. Rev. B.* **52**, 1433. https://doi.org/10.1103/physrevb.52.1433 (1995).
41. Malerba, C. et al. Absorption coefficient of bulk and thin film Cu_2O. *Sol Energy Mater. Sol Cells.* **95**, 2848. https://doi.org/10.1016/j.solmat.2011.05.047 (2011).
42. Stevanović, V., Lany, S., Zhang, X. & Zunger, A. Correcting density functional theory for accurate predictions of compound enthalpies of formation: fitted elemental-phase reference energies. *Phys. Rev. B.* **85**, 115104. https://doi.org/10.1103/PhysRevB.85.115104 (2012).
43. Peng, H., Yang, Z. H., Perdew, J. P. & Sun, J. Versatile Van der Waals density functional based on a meta-generalized gradient approximation. *Phys. Rev. X.* **6** https://doi.org/10.1103/PhysRevX.6.041005 (2016).
44. Ning, J. et al. Workhorse minimally empirical dispersion-corrected density functional with tests for weakly bound systems: r2SCAN + rVV10. *Phys. Rev. B.* **106** https://doi.org/10.1103/PhysRevB.106.075422 (2022).
45. Wang, Y. et al. Electronic structures of Cu_2O,Cu_4O_3, and CuO: a joint experimental and theoretical study. *Phys. Rev. B.* **94**, 245418. https://doi.org/10.1103/PhysRevB.94.245418 (2016).
46. Bae, S. et al. Electronic and magnetic properties of carbide MXenes—the role of electron correlations. *Mater. Today Adv.* **9** https://doi.org/10.1016/j.mtadv.2020.100118 (2021).
47. Kresse, G. & Hafner, J. Ab initio molecular dynamics for liquid metals. *Phys. Rev. B.* **47**, 558. https://doi.org/10.1103/physrevb.47.558 (1993).
48. Kresse, G. & Furthmüller, J. Efficiency of ab-initio total energy calculations for metals and semiconductors using a plane-wave basis set. *Comput. Mater. Sci.* **6**, 15. https://doi.org/10.1016/0927-0256(96)00008-0 (1996).
49. Kresse, G. & Joubert, D. From ultrasoft pseudopotentials to the projector augmented-wave method. *Phys. Rev. B.* **59**, 1758. https://doi.org/10.1103/PhysRevB.59.1758 (1999).
50. Perdew, J. P., Burke, K. & Ernzerhof, M. Generalized gradient approximation made simple. *Phys. Rev. Lett.* **77**, 3865. https://doi.org/10.1103/PhysRevLett.77.3865 (1996).
51. Sabatini, R., Gorni, T. & de Gironcoli, S. Nonlocal Van der Waals density functional made simple and efficient. *Phys. Rev. B.* **87** https://doi.org/10.1103/PhysRevB.87.041108 (2013).
52. Dudarev, S. L., Botton, G. A., Savrasov, S. Y., Humphreys, C. J. & Sutton, A. P. Electron-energy-loss spectra and the structural stability of nickel oxide: an LSDA + *U* study. *Phys. Rev. B.* **57**, 1505. https://doi.org/10.1103/PhysRevB.57.1505 (1998).
53. Monkhorst, H. J. & Pack, J. D. Special points for Brillouin-zone integrations. *Phys. Rev. B.* **13**, 5188. https://doi.org/10.1103/PhysRevB.13.5188 (1976).
54. Köhler, L. & Kresse, G. Density functional study of CO on Rh(111). *Phys. Rev. B.* **70**, 165405. https://doi.org/10.1103/PhysRevB.70.165405 (2004).

Acknowledgements

This study was supported by JSPS KAKENHI (Grant No. 23KF0030 and 23K04356) from the Japan Society for the Promotion of Science and GIMRT Program of the Institute for Materials Research, Tohoku University (202312-RDKGE-0508). This research was conducted using supercomputers at Research Center for Computational Science at ISSP and Information Technology Center, the University of Tokyo and MASAMUNE-IMR at

Institute for Materials Research, Tohoku University (Project No. 202211-SCKXX-0401).

Author contributions

S. B. and N. E. conducted the calculations, S. B., N. E., and H. R. analysed the results. S. B. and H.R. wrote the manuscript. All authors reviewed the manuscript.

Competing interests

The authors declare no competing interests.

Additional information

Supplementary Information The online version contains supplementary material available at https://doi.org/10.1038/s41598-025-92069-7.

Correspondence and requests for materials should be addressed to S.B. or H.R.

Reprints and permissions information is available at www.nature.com/reprints.

Publisher's note Springer Nature remains neutral with regard to jurisdictional claims in published maps and institutional affiliations.